Journal of Engineering and Applied Research (JEAR)

National University of Skills

Summer & Autumn 2025, Vol. 2, No. 2, p. 147- 160

Journal Homepage: https://jear.tvu.ac.ir

:10.48301/JEAR.2024.474745.1123

Transformation Behavior and Microstructural Tuning of Ni-rich NiTi Alloys with 3 at.% Hafnium Addition for High-Temperature Applications

Moharram Shameli[1*], Behzad Abasht[2], Elyas Haddadi[3], Gholamreza Hashemi[4]

[1,2,4] Space Thrusters Research Institute, Iranian Space Research Center, Tabriz, Iran

[3]Department of Mechanical Engineering, Technical and Vocational University (TVU), Tehran, Iran

ARTICLE INFO

Article Type:
Original Research

Received: 06.08.2025
Revised: 08.31.2025
Accepted: 04.11.2025

Keyword:
Shape memory Alloy
NiTiHf
Transformation Temperature
Microstructure
Wire-drawing

***Corresponding Author:**
Moharram Shameli
Email:
m.shameli@isrc.ac.ir

ABSTRACT

Shape memory alloys (SMAs), particularly NiTi-based systems, have garnered significant attention due to their exceptional functional properties, including the shape memory effect (SME) and superelasticity (SE). These characteristics can be tuned by modifying the transformation temperatures through ternary alloying. In this study, the main objective is to tune the transformation temperatures of NiTi alloys through ternary alloying by introducing a low hafnium content (3 at.%). The $Ni_{48.4}Ti_{48.6}Hf_3$ ingots were subjected to various annealing treatments to optimize microstructural homogeneity and promote controlled precipitation of secondary phase precipitation. Dilatometry revealed that annealing at 1050°C for 48 h resulted in the most favorable transformation characteristics, with martensitic start (M_s), martensitic finish (M_f), austenitic start (A_s), and austenitic finish (A_f) temperatures of approximately 65°C, 50°C, 90°C, and 110°C, respectively, measured for the homogenized sample. Transmission electron microscopy confirmed the presence of Ti_2Ni precipitates. The incorporation of Hf effectively increased the transformation temperatures, attributed to a reduction in valence electron concentration (c_v), thereby enhancing resistance to shear-induced martensitic transformation. Furthermore, mechanical testing demonstrated improved strength and thermal stability in the Hf-modified alloy compared to conventional NiTi, highlighting its suitability for high-temperature shape memory applications. Furthermore, thermomechanical processing including hot rolling, cold rolling, and wire-drawing to 0.3 mm diameter was successfully performed, confirming the alloy's processability.

E-ISSN: 3060-6357

Introduction

In recent years, lightweight elements have become increasingly vital in advanced engineering applications due to their high strength-to-weight ratio, corrosion resistance, and versatility. They are widely used in transportation, medical and dental technologies, and protective coatings, particularly nickel-based coatings [1; 2]. Equiatomic or near-equiatomic NiTi alloys are widely recognized for their shape memory effect (SME) and superelasticity (SE), making them highly suitable for diverse applications, particularly in medical and dental fields [3]. The incorporation of a third alloying element, such as hafnium (Hf), into binary NiTi alloys has been shown to significantly influence their transformation temperatures. Specifically, Hf addition is known to raise these temperatures by altering the valence electron concentration, thereby increasing resistance to shearing during martensitic transformation [4]. Among the various classes of shape memory alloys (SMAs), NiTi-based compositions are considered the most prominent due to their outstanding SME, mechanical performance, and physical properties [5; 6]. SMAs with transformation temperatures (TTs) below 100°C are commonly used in technological applications that operate at relatively low temperatures, such as biomedical implants and micro-actuators [7; 8]. In recent years, researchers have explored the substitution of Ni or Ti with a third element (such as Hf, Zr, Pt, Pd, or Au) to develop NiTi-based high-temperature shape memory alloys (HTSMAs) [9-13]. The capability of these HTSMAs to function at temperatures exceeding 100°C extends their potential use to demanding industrial environments, including the oil, aerospace, and automotive sectors. Among the various ternary additions investigated, Hf has received particular attention due to its strong effect on transformation temperatures and its relatively lower cost compared to other elements [14; 15].

Among NiTi-based ternary alloys, NiTiHf alloys are considered particularly promising due to their favorable combination of high transformation temperatures (above 100°C), relatively low cost compared to Pt- or Au-containing systems, and retention of significant shape memory effect (SME) and superelasticity (SE). However, the Ti-rich variants of these alloys introduce several drawbacks, including reduced ductility and strength, increased transformation temperature hysteresis (often exceeding 50°C), limited resistance to slip, and poor cyclic stability [16]. It has been demonstrated that thermo-mechanical processing techniques (such as grain size refinement, work hardening, and other mechanical treatments) can improve the reversibility of the transformation behavior in high-temperature SMAs (HTSMAs), including NiTiHf alloys [17-21].

NiTiHf alloys are typically manufactured in various forms such as sheets, rods, and wires. However, producing wire forms poses significant processing challenges. These include:

- The development of compressive lattice stresses in the NiTi matrix due to Hf substitution [22; 23].
- Formation of the $(Hf,Ti)_2Ni$ intermetallic phase in Ti-rich NiTiHf compositions [24; 25].
- Nanoprecipitation of the H-phase in Ni-rich NiTiHf alloys [26-28].

Such features are known to reduce ductility and promote embrittlement during processing. Furthermore, the formation of aggressive Ti- and Hf-rich surface oxides complicates processing by causing compositional instability and promoting the development of intermetallic phases beneath the oxide layer.

In this study, the processability of hot-rolled (HR) and cold-drawn $Ni_{48.4}Ti_{48.6}Hf_3$ HTSMA wires is examined, with particular focus on addressing these processing-related challenges. The investigation is structured to evaluate two primary aspects: (i) the uniformity of mechanical properties along the wire, and (ii) the transformation behavior, thermomechanical response, and SME characteristics of the HR, solution-treated, and aged $Ni_{48.4}Ti_{48.6}Hf_3$ wires.

Despite the notable advantages of NiTiHf alloys, issues related to their formability and microstructural control remain significant barriers to improved performance and broader adoption [29]. In particular, the influence of mechanical processing routes (such as hot rolling and cold drawing) on property uniformity and phase transformation behavior requires comprehensive investigation. Understanding the correlation between microstructure and thermo-mechanical performance is crucial for developing effective strategies to enhance durability, ductility, and cyclic stability, ultimately enabling the reliable use of these materials in demanding industrial applications.

Recent advancements in characterization techniques (particularly high-resolution transmission electron microscopy (HRTEM) and dilatometry) have significantly improved the precision with which microstructural features and phase transformations in NiTiHf alloys can be analyzed. These techniques offer deeper insights into the relationships between processing parameters, precipitation behavior, and key functional properties such as the shape memory effect (SME) and superelasticity (SE). As a result, tailoring heat treatment protocols and mechanical processing routes based on microstructural understanding can greatly enhance the reliability and functional performance of NiTiHf wires, especially for high-temperature applications.

This study focuses on systematically evaluating the processability of $Ni_{48.4}Ti_{48.6}Hf_3$ HTSMA wires fabricated by hot rolling and cold drawing. This work addresses major processing-related challenges, including compressive lattice stresses induced by Hf substitution in the NiTi matrix, the formation of $(Hf,Ti)_2Ni$ intermetallic phases, and nanoprecipitation of the H-phase factors that commonly result in embrittlement during deformation. By thoroughly assessing the uniformity

of mechanical properties, transformation characteristics, and thermo-mechanical response, this study offers practical insights into improving cyclic stability, durability, and the overall performance of NiTiHf alloys in elevated-temperature service environments.

Experimental method

Alloy designing

Electrovalence calculations were conducted to predict phase transformation temperatures and determine the optimal alloy composition for applications involving high mechanical loads near an austenitic finish temperature of approximately 90°C. Zarinejad et al. [4] established a correlation between electrovalence and the martensitic start temperature (M_s), and, using Equations (1) and (2), developed a concentration diagram (C_v) as a function of Ms.

$$\frac{e_V}{a} = f_{Ni}e_v^{Ti} + f_{Ti}e_v^{Ti} + f_T e_v^T + f_Q e_v^Q \quad (1)$$

$$C_v = \frac{e_v}{e_t} = \frac{x_{Ni}e_v^{Ni} + x_{Ti}e_v^{Ti} + x_{Hf}e_v^{Hf}}{x_{Ni}Z^{Ni} + x_{Ti}Z^{Ti} + x_{Hf}Z^{Hfi}} \quad (2)$$

In Equations (1) and (2), e_V/a represents the electron-to-atom ratio, C_v denotes the concentration of valence electrons, F is the molar fraction of each element, T indicates the atomic number, Q corresponds to the number of valence electrons, and Z is the total number of atoms in the formula unit. Based on the calculated values for C_v and $\frac{e_V}{a}$, a summary of which is presented in Table 1, the composition $Ni_{48.4}Ti_{48.6}Hf_3$ was identified as the optimal candidate, providing the desired transformation temperatures. It is noteworthy that, according to Karaca et al. [16], in a NiTiHf10 alloy, the martensitic start temperature (Ms) remains relatively stable as the nickel content increases. However, once the nickel content exceeds 50 atomic percent, a significant drop in MP temperature occurs. While ternary NiTi-based shape memory alloys typically incorporate more than 5 at.% Hf to achieve high transformation temperatures, the focus of this study is on developing a NiTiHf alloy with a reduced Hf content. This approach aims to balance elevated transformation temperatures with improved workability and formability.

Table 1. Calculated $\frac{e_v}{a}$ and c_v for different compounds.

Composition	Electron-to-atom ratio (*ev*/atom)	Concentration of valence electrons (C_v)
$Ni_{50}Ti_{50}$	7	0.28
$Ni_{47}Ti_{53}$	6.82	0.275
$Ni_{50}Ti_{47}Hf_3$	7	0.258
$Ni_{47}Ti_{50}Hf_3$	6.82	0.259
$Ni_{48.4}Ti_{48.6}Hf_3$	6.80	0.280

Material and fabrication process

Ingots of $Ni_{48.4}Ti_{48.6}Hf_3$ alloy were fabricated using a vacuum arc remelting (VAR) furnace with raw materials of 99.99% purity. Following casting, the ingots were subjected to annealing in a vacuum furnace at four different temperatures (1000, 1050, 1100, and 1150°C) to evaluate the effect of thermal treatment on compositional homogeneity and phase stability. This step aimed to identify the optimal annealing condition for promoting uniform microstructure while avoiding undesirable grain growth. A homogenization treatment at 1050°C for 48 hours was chosen because it offered the best balance between phase uniformity and microstructural control. Subsequently, the homogenized ingot underwent hot rolling at 1000°C, achieving an overall cross-sectional area reduction of 80%. Hot rolling was carried out starting at 1000°C, followed by successive passes at 950°C, 900°C, and 850°C, achieving an overall reduction of 80%. Following hot rolling, cold rolling was performed in a stepwise manner to further reduce the cross-sectional area by 70%. This process contributed to additional microstructural refinement, improved strength, and the elimination of residual inhomogeneities.

Inter-pass annealing was conducted between rolling steps in a resistance furnace at 800°C for 7 minutes under an argon atmosphere. A boron nitride coating was applied to the sample surfaces to prevent oxidation and preserve surface quality during heat treatment. This intermediate annealing step served to relieve internal stresses introduced during deformation and facilitated better control over the evolving microstructure [30]. For final processing, the material was subjected to wire drawing to produce wires with a target diameter of 0.3 mm. The wire drawing involved a total area reduction of 75% and was performed in multiple stages. Intermediate annealing steps were employed between drawing stages to minimize work hardening and ensure a uniform, fine-grained microstructure suitable for high-performance applications.

Characterization

Microstructural characterization was performed using both optical microscopy (OM) and scanning electron microscopy (SEM). Prior to analysis, the specimens were sectioned and prepared following standard metallographic procedures. This included sequential mechanical grinding with SiC emery papers, followed by polishing with Al_2O_3 suspension to achieve a mirror-like surface suitable for microscopic examination. The SEM used in this study was equipped with an energy-dispersive X-ray spectroscopy (EDS) detector to facilitate chemical composition analysis of both the matrix and any secondary phases present. Phase identification was conducted using X-ray diffraction (XRD) with Cu Kα radiation ($\lambda = 0.154$ nm), operating at 45 kV and 200 mA. Scans were carried out over a 2θ range of 5° to 100°, with a step size of 0.02° and a scanning speed of 2°/min. These parameters were

selected to ensure high-resolution detection of crystalline phases. For thermal analysis, cylindrical specimens with dimensions of 10 mm in length and 2 mm in diameter were prepared from the homogenized alloy and analyzed using an Adamel DT1000 dilatometer. Non-isothermal dilatometry experiments were performed up to 200°C to study the thermal expansion behavior and transformation characteristics of the material. Transmission electron microscopy (TEM) samples were prepared using conventional mechanical thinning followed by twin-jet electro-polishing. The electrolyte consisted of a 3:7 mixture of HNO_3 and C_2H_5OH. Electro-polishing was performed at -20°C with an applied voltage of 22 V to produce electron-transparent foils suitable for high-resolution microstructural analysis.

Result and discussion

Figure 1a shows an optical microscopy (OM) image of the as-cast ingot. The microstructure reveals numerous titanium-rich particles, which are further confirmed by X-ray diffraction (XRD) analysis (Figure 1b). The XRD pattern also exhibits strong peaks corresponding to the B19' martensitic phase, indicating that the ingot predominantly possesses a martensitic structure at room temperature prior to annealing. This suggests that the austenite transformation temperature (A_f) lies above ambient temperature, and thus the alloy exists in a metastable state with martensite retained at room temperature [31]. Consequently, further heat treatment is necessary to stabilize the microstructure. Additionally, a minor peak attributed to titanium oxide is observed in the XRD spectrum, implying minimal surface oxidation during processing.

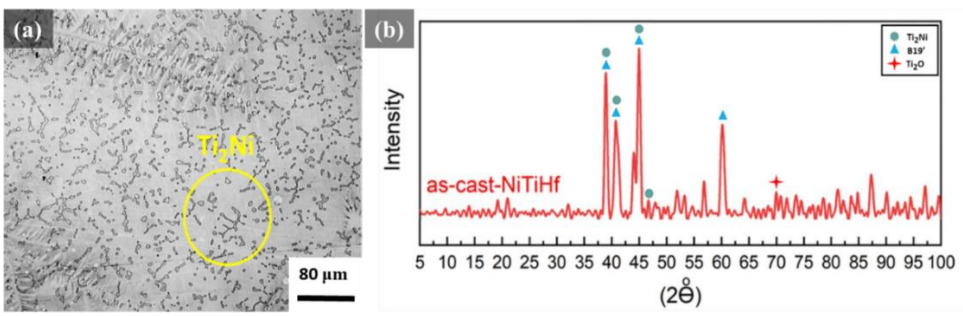

Figure 1. a) Optical microscopy (OM) image of the microstructure of as-cast ingot. b) XRD pattern of as-cast $NiTiHf_3$ ingot.

Transmission electron microscopy (TEM) of the as-cast samples reveals the presence of nanoscale Ti_2Ni precipitates embedded within the martensitic matrix. The selected area electron diffraction (SAED) pattern shown in Figure 2a confirms the crystallographic planes <211> and <134> of the B19' phase. The formation of

Ti_2Ni secondary phases may significantly affect the alloy's mechanical behavior and phase stability.

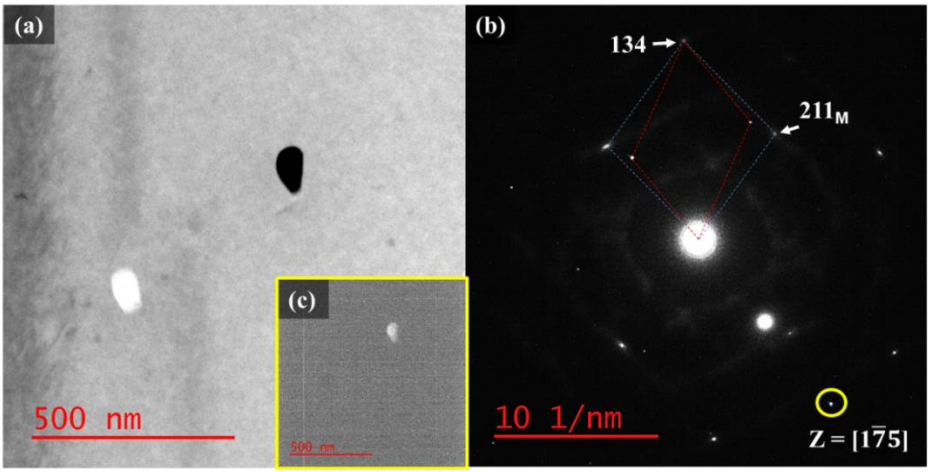

Figure 2. TEM images from as-cast sample, a) bright field image, b) SAED pattern of a, c) dark field image of the spot, which has been shown by the yellow cycle in b.

The brittleness of the as-cast ingot [32; 33] mainly arises from precipitate particles in the microstructure, which serve as stress concentrators and initiate cracking. To improve the alloy's malleability and enable subsequent wire fabrication, careful annealing at an appropriate temperature and duration is essential. For homogenization, four different temperatures were chosen, as summarized in Table 2. After two hours of heat treatment at each temperature, the phase transformation temperatures remained nearly unchanged across all conditions (Table 2). Therefore, microstructural analysis (Figure 3) was used to determine the optimal annealing temperature. The sample annealed at 1050°C exhibited the best compromise between precipitate dissolution and retention of the desired matrix phase, resulting in a microstructure suitable for improved mechanical performance and wire processing. Higher annealing temperatures of 1100°C and 1150°C showed signs of incipient melting, while the sample treated at 1000°C retained a higher density of precipitates. Considering these factors, 1050°C was selected as the ideal homogenization temperature to balance microstructural stability and processability.

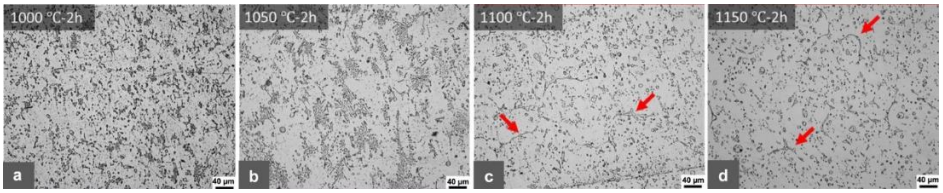

Figure 3. Optical microscopy image after two hours of annealing at temperatures a-d) 1000, 1050, 1100, and 1150˚C.

Following the identification of the optimal homogenization temperature, it was necessary to determine the appropriate annealing duration to achieve sufficient precipitate dissolution. The kinetics of homogenization play a critical role in refining the microstructure, as extended annealing promotes more complete dissolution of second-phase particles. At 1050°C, varying the homogenization time revealed a clear trend: increasing the duration led to a progressive reduction in the volume fraction of precipitates. As shown in Figure 4, extending the homogenization time from 10 to 48 hours reduced the secondary phase content from 16% to 2.3%, with 48 hours identified as the optimal annealing duration.

Table 2. The phase transformation temperatures of samples at different annealing conditions.

Condition	A_f (°C)	A_s (°C)	M_s (°C)	M_f (°C)
1000℃-2h	105	85	62	43
1050℃-2h	108	84	66	46
1100℃-2h	110	86	68	50
1150℃-2h	**105**	**80**	**61**	**40**

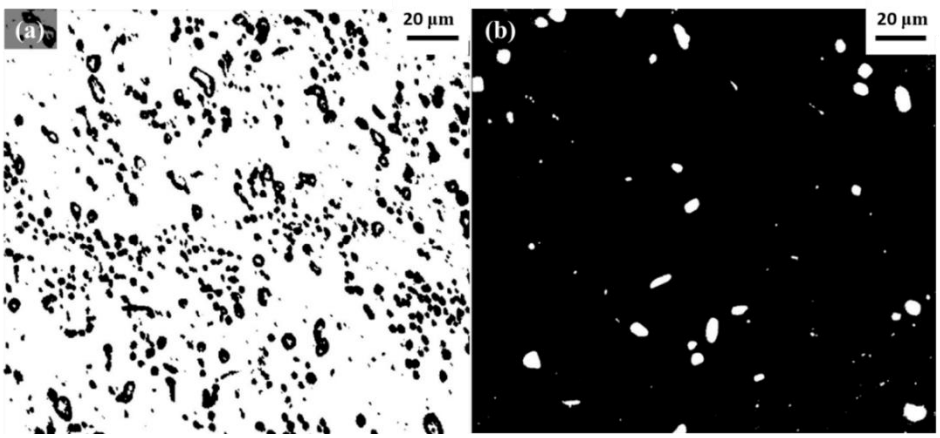

Figure 4. Image analysis of the annealed sample in 1050℃ for a) 10 h, b) 48 h.

Energy-dispersive spectroscopy (EDS) mapping of the alloy after optimal annealing conditions revealed that the yellow-circled regions in Figure 5 are predominantly composed of HfO_2. These oxides are attributed to hafnium oxidation during high-temperature processing, a typical occurrence during prolonged thermal exposure. The presence of HfO_2 was further confirmed by X-ray diffraction (XRD) analysis, as illustrated in Figure 6. Additionally, the XRD patterns confirm that the

$Ni_{48.4}Ti_{48.6}Hf_3$ alloy retains a martensitic structure at room temperature, which is consistent with the predicted transformation temperatures.

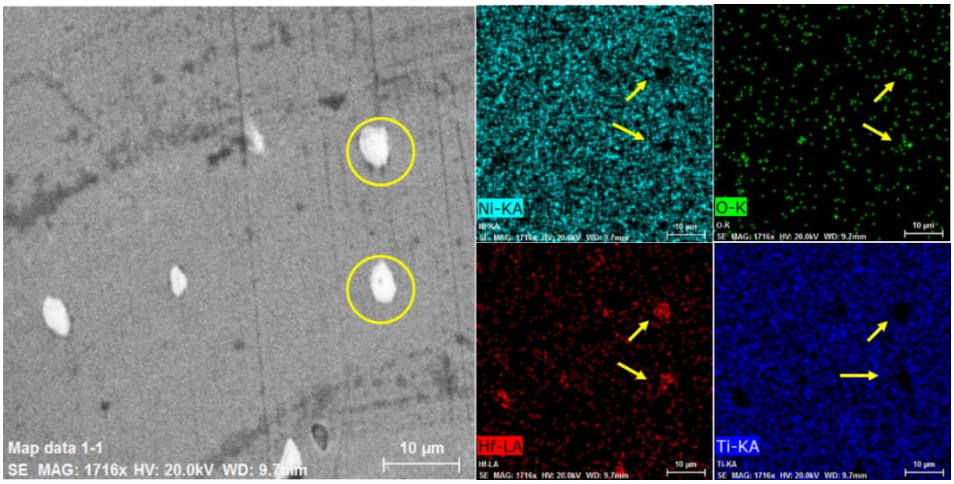

Figure 5. EDS map of the alloy annealed at 1050°C for 48 h. The yellow-circled regions correspond to HfO_2 precipitates. (Note: Scale bar corresponds to 10 µm).

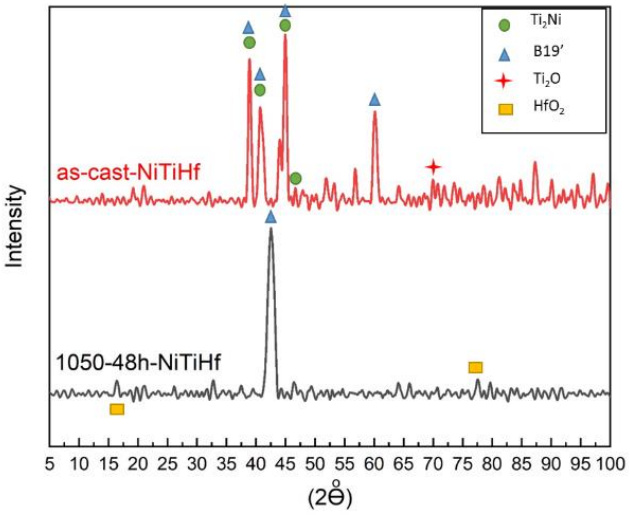

Figure 6. XRD results of as-cast and annealed samples.

The presence of Ti_2Ni precipitates is known to act as nucleation centers during martensitic transformation, thereby influencing transformation temperatures and slightly reducing ductility. HfO_2 particles mainly act as barriers to twin motion and dislocation glide, which contributes to increased strength but reduces ductility. In our alloy, the combined effect of Ti_2Ni and HfO_2 resulted in improved high-

temperature stability and strength, while wire-drawing helped distribute these phases more uniformly, reducing their embrittling effect.

Dilatometry results from the homogenized sample (Figure 7a) show elevated phase transformation temperatures. The martensitic transformation starts at 65°C (M□) and completes at 50°C (M_f), while the austenitic transformation initiates at 90°C (A□) and concludes at 110°C (A_f). These values align well with both XRD and transmission electron microscopy (TEM) observations, confirming the thermal stability of the martensitic phase and the functional transformation range of the alloy. Upon short-term aging at 400°C for 2 hours and 800°C for 5 minutes, the martensitic start and finish temperatures increased slightly to M_s = 67°C and M_f = 52°C, with austenitic transformation temperatures shifting to A_s = 97°C and A_f = 108°C, respectively. Following wire fabrication to a final diameter of 0.3 mm, the alloy's microstructure was re-evaluated. As shown in Figure 8, the precipitates became elongated and aligned in the direction of wire drawing. This directional distribution indicates that the wire drawing process significantly influences the morphology and orientation of second-phase particles [34], which in turn affects the mechanical and functional properties of the final product.

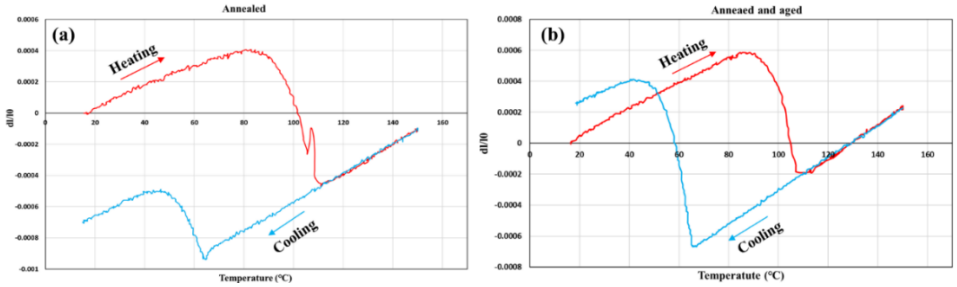

Figure 7. a) Dilatometry result for annealed sample, b) annealed and aged sample.

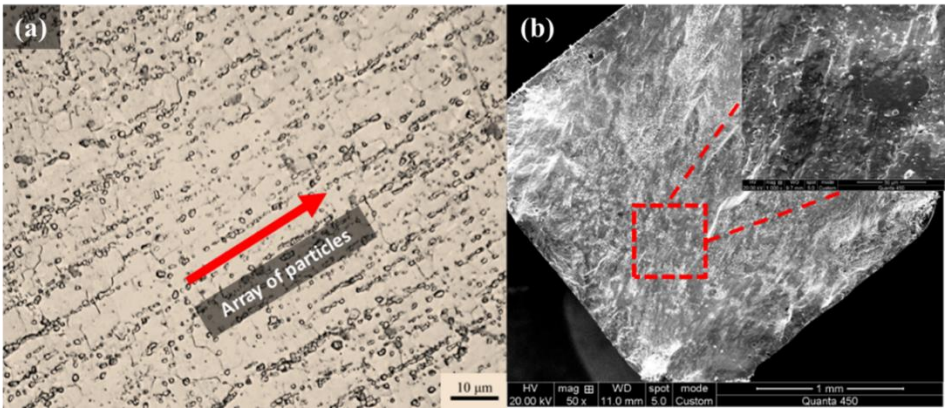

Figure 8. a) Optical microscopy image from wire with diameter 0.3 mm b) SEM fractography image from wire with diameter 2.5 mm.

Conclusion

In this study, a ternary NiTi-based shape memory alloy containing 3 at.% Hf ($Ni_{48.4}Ti_{48.6}Hf_3$) was successfully designed and cast. Comprehensive microstructural characterization of the as-cast ingot revealed the presence of Ti_2Ni precipitates and a martensitic matrix, as confirmed by TEM imaging, SAED patterns, and XRD analysis. To improve homogeneity and reduce brittleness, the ingot was homogenized at 1050°C for 48 hours under vacuum conditions, which was identified as the optimal heat treatment based on phase stability and microstructural evolution. Subsequent processing included hot and cold rolling followed by wire drawing, yielding a final wire diameter of 0.3 mm. Microstructural examination of the fabricated wire confirmed the absence of microcracks and a refined, aligned second-phase morphology, indicative of effective thermomechanical processing. Dilatometry tests demonstrated that the homogenized alloy exhibited austenite start temperatures (A_s) exceeding 85°C, confirming its suitability for high-temperature applications. Additionally, aging treatments led to a slight increase in transformation temperatures, further stabilizing the martensitic phase. Mechanical testing of the final wire showed enhanced strength and ductility relative to the as-cast condition, evidencing the successful mitigation of embrittlement typically observed in NiTiHf systems. Overall, the combined approach of controlled alloy design, optimized heat treatment, and tailored mechanical processing resulted in a $Ni_{48.4}Ti_{48.6}Hf_3$ alloy with favorable transformation characteristics, improved mechanical performance, and high structural integrity. Overall, the alloy demonstrates favorable transformation characteristics, improved mechanical performance, and high structural integrity, confirming its potential for high-temperature shape memory applications. While reliable actuation and fatigue resistance are expected, further experimental validation is required and will be considered in future studies.

Disclosure statement and funding

The authors declare no potential conflicts of interest. The present study received financial support from Iranian Space Research Center.

References

[1] Amanollahi, A., Raeissi, M., Saeidi, N., & Ebrahimzadeh, I. (2023). Evaluation of the Effect of Heat Treatment Parameters on Mechanical Properties of Architectured Steel Incorporated Low Carbon Steel and Aluminum 6061 [Evaluation of the Effect of Heat Treatment Parameters on Mechanical Properties of Architectured Steel Incorporated Low Carbon Steel and Aluminum 6061]. *Karafan Journal*, *20*(1), 279-300. https://doi.org/10.48301/kssa.2022.326385.1973

[2] Mirzamohammadi, S., Hashemi, J., & Zal, V. (2024). Modification of nanoparticle absorption using Sodium dodecyl sulfate addition in composite plating bath. *Journal of Engineering and Applied Research*, *1*(2), 91-100. https://doi.org/10.48301/jear.2024.459185.1028 (in persian)

[3] Behvar, A., Sojoodi, M., Celebi, A., & Elahinia, M. (2025). Insights into the Future of Manufacturing and Designing NiTi-Cu Shape Memory Alloys with Powder Sintering-Based Process Binder Jet Additive Manufacturing: A Short Review. *Shape Memory and Superelasticity*. https://doi.org/10.1007/s40830-025-00538-9

[4] Zarinejad, M., & Liu, Y. (2008). Dependence of transformation temperatures of NiTi-based shape-memory alloys on the number and concentration of valence electrons. *Advanced Functional Materials*, *18*(18), 2789-2794. https:/doi.org/10.1002/adfm.200701423

[5] Khoo, Z. X., An, J., Chua, C. K., Shen, Y. F., Kuo, C. N., & Liu, Y. (2018). Effect of heat treatment on repetitively scanned SLM NiTi shape memory alloy. *Materials*, *12*(1), 77. https:/doi.org/10.3390/ma12010077

[6] Kumar, P., & Lagoudas, D. (2008). Introduction to shape memory alloys. In *Shape memory alloys: modeling and engineering applications* (1-51). Springer. https://doi.org/10.1007/978-0-387-47685-8_1

[7] Dai Hsu, D. H., Hornbuckle, B. C., Valderrama, B., Barrie, F., Henderson, H. B., Thompson, G. B., & Manuel, M. V. (2015). The effect of aluminum additions on the thermal, microstructural, and mechanical behavior of NiTiHf shape memory alloys. *Journal of Alloys and Compounds*, *638*, 67-76. https://doi.org/10.1016/j.jallcom.2015.01.071

[8] Júnior, M. L. L., Pino, L., Barati, M., Saint-Sulpice, L., Daniel, L., & Chirani, S. A. (2025). Design of SMA wire based actuators: A phase transformation and electric coupling parametric study. *Sensors and Actuators A: Physical*, 116255. https://doi.org/10.1016/j.sna.2025.116255

[9] Benafan, O., Gaydosh, D., Noebe, R., Qiu, S., & Vaidyanathan, R. (2016). In situ neutron diffraction study of NiTi–21Pt high-temperature shape memory alloys. *Shape Memory and Superelasticity*, *2*, 337-346. https://doi.org/10.1007/s40830-016-0095-7

[10] Casalena, L., Bigelow, G. S., Gao, Y., Benafan, O., Noebe, R. D., Wang, Y., & Mills, M. J. (2017). Mechanical behavior and microstructural analysis of NiTi-40Au shape memory alloys exhibiting work output above 400 C. *Intermetallics*, *86*, 33-44. https://doi.org/10.1016/j.intermet.2017.03.005

[11] Casalena, L., Coughlin, D., Yang, F., Chen, X., Paranjape, H., Gao, Y., Noebe, R., Bigelow, G., Gaydosh, D., & Padula, S. (2015). Transformation and deformation characterization of NiTiHf and NiTiAu high temperature shape memory alloys. *Microscopy and Microanalysis*, *21*(S3), 607-608. https://doi.org/10.1017/S1431927615003839

[12] Evirgen, A., Karaman, I., Pons, J., Santamarta, R., & Noebe, R. (2016). Role of nano-precipitation on the microstructure and shape memory characteristics of a new Ni50. 3Ti34. 7Zr15 shape memory alloy. *Materials Science and Engineering: A*, *655*, 193-203. https://doi.org/10.1016/j.msea.2015.12.076

[13] Inamura, T., Takahashi, Y., Hosoda, H., Wakashima, K., Nagase, T., Nakano, T., Umakoshi, Y., & Miyazaki, S. (2006). Martensitic Transformation Behavior and Shape Memory Properties of Ti–Ni–Pt Melt-Spun Ribbons. *Materials transactions*, *47*(3), 540-545. https://doi.org/10.2320/matertrans.47.540

[14] Benafan, O., Garg, A., Noebe, R., Bigelow, G., Padula Ii, S., Gaydosh, D., Schell, N., Mabe, J., & Vaidyanathan, R. (2014). Mechanical and functional behavior of a Ni-rich Ni50. 3Ti29. 7Hf20 high temperature shape memory alloy. *Intermetallics*, *50*, 94-107. https://doi.org/10.1016/j.intermet.2014.02.006

[15] Elsayed, A., Guleria, T., Tian, H., Sahu, B. P., Atli, K. C., Olleak, A., Elwany, A., Arroyave, R., Lagoudas, D., & Karaman, I. (2025). Functionally Graded NiTiHf High-Temperature Shape Memory Alloys Using Laser Powder Bed Fusion: Localized Phase Transformation Control and Multi-Stage Actuation. *Acta Materialia*, 121175. https://doi.org/10.1016/j.actamat.2025.121175

[16] Karaca, H., Saghaian, S., Ded, G., Tobe, H., Basaran, B., Maier, H., Noebe, R., & Chumlyakov, Y. (2013). Effects of nanoprecipitation on the shape memory and material properties of an Ni-rich NiTiHf high temperature shape memory alloy. *Acta Materialia*, *61*(19), 7422-7431. https://doi.org/10.1016/j.actamat.2013.08.048

[17] Evirgen, A., Karaman, I., Santamarta, R., Pons, J., & Noebe, R. (2015). Microstructural characterization and shape memory characteristics of the Ni50. 3Ti34. 7Hf15 shape memory alloy. *Acta Materialia*, *83*, 48-60. https://doi.org/10.1016/j.actamat.2014.09.027

[18] Noorabadi, S. S. H., & Nili-Ahmadabadi, M. (2019). Influence of Hf Solute Addition on the Shape Memory and Superelastic Behavior of NiTi Alloy. *Metallurgical Engineering*, *22*(3), 168-177. https://doi.org/10.22076/me.2019.104593.1235

[19] Saghaian, S., Karaca, H., Souri, M., Turabi, A., & Noebe, R. (2016). Tensile shape memory behavior of Ni50. 3Ti29. 7Hf20 high temperature shape memory alloys. *Materials & Design*, *101*, 340-345. https://doi.org/10.1016/j.matdes.2016.03.163

[20] Santamarta, R., Arróyave, R., Pons, J., Evirgen, A., Karaman, I., Karaca, H., & Noebe, R. (2013). TEM study of structural and microstructural characteristics of a precipitate phase in Ni-rich Ni–Ti–Hf and Ni–Ti–Zr shape memory alloys. *Acta Materialia*, *61*(16), 6191-6206. https://doi.org/10.1016/j.actamat.2013.06.057

[21] Wu, Y., Patriarca, L., Sehitoglu, H., & Chumlyakov, Y. (2016). Ultrahigh tensile transformation strains in new Ni50. 5Ti36. 2Hf13. 3 shape memory alloy. *Scripta Materialia*, *118*, 51-54. https://doi.org/10.1016/j.scriptamat.2016.03.009

[22] Kirmacioglu, K., Kaynak, Y., & Benafan, O. (2019). Machinability of Ni-rich NiTiHf high temperature shape memory alloy. *Smart Materials and Structures*, *28*(5), 055008. https://doi.org/10.1088/1361-665X/ab02a2

[23] Volodko, S., Yudin, S., Korotitskiy, A., Markova, G., Cheverikin, V., Permyakova, D., Poliakov, M., Titov, D., Moskovkikh, D., & Kasimtsev, A. (2024). Hot deformation behavior of NiTiHf alloy under compression: Effect of deformation heating on flow softening. *Materials Characterization*, *212*, 113981. https://doi.org/10.1016/j.matchar.2024.113981

[24] Belbasi, M., & Salehi, M. T. (2014). Influence of chemical composition and melting process on hot rolling of NiTiHf shape memory alloy. *Journal of materials engineering and performance*, *23*, 2368-2372. https://doi.org/10.1007/s11665-014-1006-8

[25] Javadi, M. M., Belbasi, M., Salehi, M. T., & Afshar, M. R. (2011). Effect of aging on the microstructure and shape memory effect of a hot-rolled NiTiHf alloy. *Journal of materials engineering and performance*, *20*, 618-622. https://doi.org/10.1007/s11665-011-9885-4

[26] Amin-Ahmadi, B., Pauza, J. G., Shamimi, A., Duerig, T. W., Noebe, R. D., & Stebner, A. P. (2018). Coherency strains of H-phase precipitates and their influence on functional properties of nickel-titanium-hafnium shape memory alloys. *Scripta Materialia*, *147*, 83-87. https://doi.org/10.1016/j.scriptamat.2018.01.005

[27] Gantz, F., Cooper, S. R., Smith, J. D., & Young, M. L. (2024). Compositional Changes of H-phase Precipitates in NiTiHf Shape Memory Alloys using Atom Probe

Tomography. *Scripta Materialia*, *250*, 116167. https://doi.org/10.1016/j.scriptamat.2024.116167

[28] Hornbuckle, B., Noebe, R., & Thompson, G. (2015). Influence of Hf solute additions on the precipitation and hardenability in Ni-rich NiTi alloys. *Journal of Alloys and Compounds*, *640*, 449-454. https://doi.org/10.1016/j.jallcom.2015.04.002

[29] Kim, W.-C., Lim, K.-R., Kim, W.-T., Park, E.-S., & Kim, D.-H. (2022). Recent advances in multicomponent NiTi-based shape memory alloy using metallic glass as a precursor. *Progress in Materials Science*, *123*, 100855. https://doi.org/10.1016/j.pmatsci.2021.100855

[30] Ahmad, S., Hashmi, A. W., Singh, J., Arora, K., Tian, Y., Iqbal, F., Al-Dossari, M., & Khan, M. I. (2024). Innovations in additive manufacturing of shape memory alloys: alloys, microstructures, treatments, applications. *Journal of Materials Research and Technology*. https://doi.org/10.1016/j.jmrt.2024.08.213

[31] Mabruri, E., Sriyono, B., Adjiantoro, B., & Adnyana, D. (2016). Pengaruh Solution Annealing Dan Aging Pada Kawat Paduan Shape Memory Ni-Ti Dan Ni-Ti-Cu. In: Metalurgi. DOI:10.14203/metalurgi.v27i2.142

[32] Benafan, O., Bigelow, G., Garg, A., Noebe, R., Gaydosh, D., & Rogers, R. (2021). Processing and scalability of NiTiHf high-temperature shape memory alloys. *Shape Memory and Superelasticity*, *7*, 109-165. https://doi.org/10.1007/s40830-020-00306-x

[33] Karaca, H., Acar, E., Tobe, H., & Saghaian, S. (2014). NiTiHf-based shape memory alloys. *Materials Science and Technology*, *30*(13), 1530-1544. https://doi.org/10.1179/1743284714Y.0000000598

[34] Zhou, S., Chen, T., Mi, B., Ma, X., Wang, J., Jin, M., Liu, P., Liaw, P. K., & Li, W. (2025). Recent progress in microstructures and properties of NiTiTa complex materials for biomedical applications. *Journal of Materials Research and Technology*. https://doi.org/10.1016/j.jmrt.2025.03.054